EUROPEAN LABORATORY FOR PARTICLE PHYSICS

CERN-PPE/96-150
17 October 1996

Measurements of $|V_{\rm cb}|$, form factors and branching fractions in the decays $\overline{\rm B}^0 \to {\rm D}^{*+}\ell^-\overline{\nu}_\ell$ and $\overline{\rm B}^0 \to {\rm D}^{+}\ell^-\overline{\nu}_\ell$

The ALEPH Collaboration [1]

Abstract

Two samples of exclusive semileptonic decays, 579 $\overline{\rm B}^0 \to {\rm D}^{*+}\ell^-\overline{\nu}_\ell$ events and 261 $\overline{\rm B}^0 \to {\rm D}^{+}\ell^-\overline{\nu}_\ell$ events, are selected from approximately 3.9 million hadronic Z decays collected by the ALEPH detector at LEP. From the reconstructed differential decay rate of each sample, the product of the hadronic form factor $\mathcal{F}(\omega)$ at zero recoil of the ${\rm D}^{(*)+}$ meson and the CKM matrix element $|V_{\rm cb}|$ are measured to be

$$\begin{aligned} \mathcal{F}_{\rm D^{*+}}(1)|V_{\rm cb}| &= (31.9 \pm 1.8_{\rm stat} \pm 1.9_{\rm syst}) \times 10^{-3}, \\ \mathcal{F}_{\rm D^{+}}(1)|V_{\rm cb}| &= (27.8 \pm 6.8_{\rm stat} \pm 6.5_{\rm syst}) \times 10^{-3}. \end{aligned}$$

The ratio of the form factors $\mathcal{F}_{\rm D^+}(1)$ and $\mathcal{F}_{\rm D^{*+}}(1)$ is measured to be

$$\mathcal{F}_{\rm D^+}(1)/\mathcal{F}_{\rm D^{*+}}(1) = 0.87 \pm 0.22_{\rm stat} \pm 0.21_{\rm syst}.$$

A value of $|V_{\rm cb}|$ is extracted from the two samples, using theoretical constraints on the slope and curvature of the hadronic form factors and their normalization at zero recoil, with the result

$$|V_{\rm cb}| = (34.4 \pm 1.6_{\rm stat} \pm 2.3_{\rm syst} \pm 1.4_{\rm th}) \times 10^{-3}.$$

The branching fractions are measured from the two integrated spectra to be

$$\begin{aligned} {\rm Br}(\overline{\rm B}^0 \to {\rm D}^{*+}\ell^-\overline{\nu}_\ell) &= (5.53 \pm 0.26_{\rm stat} \pm 0.52_{\rm syst})\%, \\ {\rm Br}(\overline{\rm B}^0 \to {\rm D}^{+}\ell^-\overline{\nu}_\ell) &= (2.35 \pm 0.20_{\rm stat} \pm 0.44_{\rm syst})\%. \end{aligned}$$

(Submitted to Physics Letters B)

[1] See the following pages for the list of authors

The ALEPH Collaboration

D. Buskulic, I. De Bonis, D. Decamp, P. Ghez, C. Goy, J.-P. Lees, A. Lucotte, M.-N. Minard, J.-Y. Nief, P. Odier, B. Pietrzyk

Laboratoire de Physique des Particules (LAPP), IN^{2}P^3-CNRS, 74019 Annecy-le-Vieux Cedex, France

M.P. Casado, M. Chmeissani, P. Comas, J.M. Crespo, M. Delfino, I. Efthymiopoulos,[1] E. Fernandez, M. Fernandez-Bosman, Ll. Garrido,[15] A. Juste, M. Martinez, S. Orteu, C. Padilla, I.C. Park, A. Pascual, J.A. Perlas, I. Riu, F. Sanchez, F. Teubert

Institut de Fisica d'Altes Energies, Universitat Autonoma de Barcelona, 08193 Bellaterra (Barcelona), Spain[7]

A. Colaleo, D. Creanza, M. de Palma, G. Gelao, M. Girone, G. Iaselli, G. Maggi, M. Maggi, N. Marinelli, S. Nuzzo, A. Ranieri, G. Raso, F. Ruggieri, G. Selvaggi, L. Silvestris, P. Tempesta, A. Tricomi,[3] G. Zito

Dipartimento di Fisica, INFN Sezione di Bari, 70126 Bari, Italy

X. Huang, J. Lin, Q. Ouyang, T. Wang, Y. Xie, R. Xu, S. Xue, J. Zhang, L. Zhang, W. Zhao

Institute of High-Energy Physics, Academia Sinica, Beijing, The People's Republic of China[8]

D. Abbaneo, R. Alemany, A.O. Bazarko, P. Bright-Thomas, M. Cattaneo, F. Cerutti, P. Coyle, H. Drevermann, R.W. Forty, M. Frank, R. Hagelberg, J. Harvey, P. Janot, B. Jost, E. Kneringer, J. Knobloch, I. Lehraus, G. Lutters, P. Mato, A. Minten, R. Miquel, Ll.M. Mir,[2] L. Moneta, T. Oest,[20] A. Pacheco, J.-F. Pusztaszeri, F. Ranjard, P. Rensing,[12] G. Rizzo, L. Rolandi, D. Schlatter, M. Schmelling,[24] M. Schmitt, O. Schneider, W. Tejessy, I.R. Tomalin, A. Venturi, H. Wachsmuth, A. Wagner

European Laboratory for Particle Physics (CERN), 1211 Geneva 23, Switzerland

Z. Ajaltouni, A. Barrès, C. Boyer, A. Falvard, P. Gay, C. Guicheney, P. Henrard, J. Jousset, B. Michel, S. Monteil, J-C. Montret, D. Pallin, P. Perret, F. Podlyski, J. Proriol, P. Rosnet, J.-M. Rossignol

Laboratoire de Physique Corpusculaire, Université Blaise Pascal, IN^{2}P^3-CNRS, Clermont-Ferrand, 63177 Aubière, France

T. Fearnley, J.B. Hansen, J.D. Hansen, J.R. Hansen, P.H. Hansen, B.S. Nilsson, B. Rensch, A. Wäänänen

Niels Bohr Institute, 2100 Copenhagen, Denmark[9]

A. Kyriakis, C. Markou, E. Simopoulou, I. Siotis, A. Vayaki, K. Zachariadou

Nuclear Research Center Demokritos (NRCD), Athens, Greece

A. Blondel, G. Bonneaud, J.C. Brient, P. Bourdon, A. Rougé, M. Rumpf, A. Valassi,[6] M. Verderi, H. Videau[21]

Laboratoire de Physique Nucléaire et des Hautes Energies, Ecole Polytechnique, IN^{2}P^3-CNRS, 91128 Palaiseau Cedex, France

D.J. Candlin, M.I. Parsons

Department of Physics, University of Edinburgh, Edinburgh EH9 3JZ, United Kingdom[10]

E. Focardi,[21] G. Parrini

Dipartimento di Fisica, Università di Firenze, INFN Sezione di Firenze, 50125 Firenze, Italy

M. Corden, C. Georgiopoulos, D.E. Jaffe

Supercomputer Computations Research Institute, Florida State University, Tallahassee, FL 32306-4052, USA [13,14]

A. Antonelli, G. Bencivenni, G. Bologna,[4] F. Bossi, P. Campana, G. Capon, D. Casper, V. Chiarella, G. Felici, P. Laurelli, G. Mannocchi,[5] F. Murtas, G.P. Murtas, L. Passalacqua, M. Pepe-Altarelli

Laboratori Nazionali dell'INFN (LNF-INFN), 00044 Frascati, Italy

L. Curtis, S.J. Dorris, A.W. Halley, I.G. Knowles, J.G. Lynch, V. O'Shea, C. Raine, J.M. Scarr, K. Smith, P. Teixeira-Dias, A.S. Thompson, E. Thomson, F. Thomson, R.M. Turnbull

Department of Physics and Astronomy, University of Glasgow, Glasgow G12 8QQ,United Kingdom[10]

U. Becker, C. Geweniger, G. Graefe, P. Hanke, G. Hansper, V. Hepp, E.E. Kluge, A. Putzer, M. Schmidt, J. Sommer, H. Stenzel, K. Tittel, S. Werner, M. Wunsch

Institut für Hochenergiephysik, Universität Heidelberg, 69120 Heidelberg, Fed. Rep. of Germany[16]

R. Beuselinck, D.M. Binnie, W. Cameron, P.J. Dornan, E.B. Martin, A. Moutoussi, J. Nash, J.K. Sedgbeer, A.M. Stacey, M.D. Williams

Department of Physics, Imperial College, London SW7 2BZ, United Kingdom[10]

G. Dissertori, P. Girtler, D. Kuhn, G. Rudolph

Institut für Experimentalphysik, Universität Innsbruck, 6020 Innsbruck, Austria[18]

A.P. Betteridge, C.K. Bowdery, P. Colrain, G. Crawford, A.J. Finch, F. Foster, G. Hughes, T. Sloan, M.I. Williams

Department of Physics, University of Lancaster, Lancaster LA1 4YB, United Kingdom[10]

A. Galla, I. Giehl, A.M. Greene, C. Hoffmann, K. Jakobs, K. Kleinknecht, G. Quast, B. Renk, E. Rohne, H.-G. Sander, P. van Gemmeren, C. Zeitnitz

Institut für Physik, Universität Mainz, 55099 Mainz, Fed. Rep. of Germany[16]

J.J. Aubert,[21] A.M. Bencheikh, C. Benchouk, A. Bonissent, G. Bujosa, D. Calvet, J. Carr, C. Diaconu, F. Etienne, N. Konstantinidis, P. Payre, D. Rousseau, M. Talby, A. Sadouki, M. Thulasidas, K. Trabelsi

Centre de Physique des Particules, Faculté des Sciences de Luminy, IN^{2}P^3-CNRS, 13288 Marseille, France

M. Aleppo, F. Ragusa[21]

Dipartimento di Fisica, Università di Milano e INFN Sezione di Milano, 20133 Milano, Italy

R. Berlich, W. Blum, V. Büscher, H. Dietl, F. Dydak,[21] G. Ganis, C. Gotzhein, H. Kroha, G. Lütjens, G. Lutz, W. Männer, H.-G. Moser, R. Richter, A. Rosado-Schlosser, S. Schael, R. Settles, H. Seywerd, R. St. Denis, H. Stenzel, W. Wiedenmann, G. Wolf

Max-Planck-Institut für Physik, Werner-Heisenberg-Institut, 80805 München, Fed. Rep. of Germany[16]

J. Boucrot, O. Callot, Y. Choi,[26] A. Cordier, M. Davier, L. Duflot, J.-F. Grivaz, Ph. Heusse, A. Höcker, A. Jacholkowska, M. Jacquet, D.W. Kim,[19] F. Le Diberder, J. Lefrançois, A.-M. Lutz, I. Nikolic, H.J. Park,[19] M.-H. Schune, S. Simion, J.-J. Veillet, I. Videau, D. Zerwas

Laboratoire de l'Accélérateur Linéaire, Université de Paris-Sud, IN^{2}P^3-CNRS, 91405 Orsay Cedex, France

P. Azzurri, G. Bagliesi, G. Batignani, S. Bettarini, C. Bozzi, G. Calderini, M. Carpinelli, M.A. Ciocci, V. Ciulli, R. Dell'Orso, R. Fantechi, I. Ferrante, L. Foà,[1] F. Forti, A. Giassi, M.A. Giorgi, A. Gregorio, F. Ligabue, A. Lusiani, P.S. Marrocchesi, A. Messineo, F. Palla, G. Sanguinetti, A. Sciabà, P. Spagnolo, J. Steinberger, R. Tenchini, G. Tonelli,[25] C. Vannini, P.G. Verdini

Dipartimento di Fisica dell'Università, INFN Sezione di Pisa, e Scuola Normale Superiore, 56010 Pisa, Italy

G.A. Blair, L.M. Bryant, J.T. Chambers, Y. Gao, M.G. Green, T. Medcalf, P. Perrodo, J.A. Strong, J.H. von Wimmersperg-Toeller

Department of Physics, Royal Holloway & Bedford New College, University of London, Surrey TW20 OEX, United Kingdom[10]

D.R. Botterill, R.W. Clifft, T.R. Edgecock, S. Haywood, P. Maley, P.R. Norton, J.C. Thompson, A.E. Wright

Particle Physics Dept., Rutherford Appleton Laboratory, Chilton, Didcot, Oxon OX11 OQX, United Kingdom[10]

B. Bloch-Devaux, P. Colas, S. Emery, W. Kozanecki, E. Lançon, M.C. Lemaire, E. Locci, P. Perez, J. Rander, J.-F. Renardy, A. Roussarie, J.-P. Schuller, J. Schwindling, A. Trabelsi, B. Vallage

CEA, DAPNIA/Service de Physique des Particules, CE-Saclay, 91191 Gif-sur-Yvette Cedex, France[17]

S.N. Black, J.H. Dann, R.P. Johnson, H.Y. Kim, A.M. Litke, M.A. McNeil, G. Taylor

Institute for Particle Physics, University of California at Santa Cruz, Santa Cruz, CA 95064, USA[22]

C.N. Booth, R. Boswell, C.A.J. Brew, S. Cartwright, F. Combley, A. Koksal, M. Letho, W.M. Newton, J. Reeve, L.F. Thompson

Department of Physics, University of Sheffield, Sheffield S3 7RH, United Kingdom[10]

A. Böhrer, S. Brandt, G. Cowan, C. Grupen, J. Minguet-Rodriguez, F. Rivera, P. Saraiva, L. Smolik, F. Stephan,

Fachbereich Physik, Universität Siegen, 57068 Siegen, Fed. Rep. of Germany[16]

M. Apollonio, L. Bosisio, R. Della Marina, G. Giannini, B. Gobbo, G. Musolino

Dipartimento di Fisica, Università di Trieste e INFN Sezione di Trieste, 34127 Trieste, Italy

J. Rothberg, S. Wasserbaech

Experimental Elementary Particle Physics, University of Washington, WA 98195 Seattle, U.S.A.

S.R. Armstrong, P. Elmer, Z. Feng,[27] D.P.S. Ferguson, Y.S. Gao,[28] S. González, J. Grahl, T.C. Greening, O.J. Hayes, H. Hu, P.A. McNamara III, J.M. Nachtman, W. Orejudos, Y.B. Pan, Y. Saadi, I.J. Scott, A.M. Walsh,[23] J. Walsh, Sau Lan Wu, X. Wu, J.M. Yamartino, M. Zheng, G. Zobernig

Department of Physics, University of Wisconsin, Madison, WI 53706, USA[11]

---

[1]Now at CERN, 1211 Geneva 23, Switzerland.

[2]Supported by Dirección General de Investigación Científica y Técnica, Spain.

[3]Also at Dipartimento di Fisica, INFN, Sezione di Catania, Catania, Italy.

[4]Also Istituto di Fisica Generale, Università di Torino, Torino, Italy.

[5]Also Istituto di Cosmo-Geofisica del C.N.R., Torino, Italy.

[6]Supported by the Commission of the European Communities, contract ERBCHBICT941234.

[7]Supported by CICYT, Spain.

[8]Supported by the National Science Foundation of China.

[9]Supported by the Danish Natural Science Research Council.

[10]Supported by the UK Particle Physics and Astronomy Research Council.

[11]Supported by the US Department of Energy, grant DE-FG0295-ER40896.

[12]Now at Dragon Systems, Newton, MA 02160, U.S.A.

[13]Supported by the US Department of Energy, contract DE-FG05-92ER40742.

[14]Supported by the US Department of Energy, contract DE-FC05-85ER250000.

[15]Permanent address: Universitat de Barcelona, 08208 Barcelona, Spain.

[16]Supported by the Bundesministerium für Bildung, Wissenschaft, Forschung und Technologie, Fed. Rep. of Germany.

[17]Supported by the Direction des Sciences de la Matière, C.E.A.

[18]Supported by Fonds zur Förderung der wissenschaftlichen Forschung, Austria.

[19]Permanent address: Kangnung National University, Kangnung, Korea.

[20]Now at DESY, Hamburg, Germany.

[21]Also at CERN, 1211 Geneva 23, Switzerland.

[22]Supported by the US Department of Energy, grant DE-FG03-92ER40689.

[23]Now at Rutgers University, Piscataway, NJ 08855-0849, U.S.A.

[24]Now at Max-Plank-Institüt für Kernphysik, Heidelberg, Germany.

[25]Also at Istituto di Matematica e Fisica, Università di Sassari, Sassari, Italy.

[26]Permanent address: Sung Kyun Kwan University, Suwon, Korea.

[27]Now at The Johns Hopkins University, Baltimore, MD 21218, U.S.A.

[28]Now at Harvard University, Cambridge, MA 02138, U.S.A.

1 Introduction

The Heavy Quark Effective Theory (HQET) is a well established theoretical framework in which heavy hadron properties and related observables can be studied reliably in a well defined limit of QCD [1, 2, 3]. HQET relates all hadronic form factors in B semileptonic decays to a single universal form factor, the Isgur-Wise function, and fixes its normalization at zero recoil of the charm meson. This property allows for an almost model-independent determination of the CKM matrix element $|V_{\rm cb}|$ from the study of exclusive semileptonic B meson decays.

To date all measurements of $|V_{\rm cb}|$ based on exclusive semileptonic B decays have been performed from the differential decay rate of $\overline{\rm B}^0 \to {\rm D}^{*+}\ell^-\overline{\nu}_\ell$ [4, 5, 6, 7]. In the limit of zero lepton mass, the differential decay rate is:

$$\frac{{\rm d}\Gamma_{{\rm D}^{*+}}}{{\rm d}\omega}(\omega) \;=\; \frac{{\rm G_F^2}}{48\pi^3} m^3_{{\rm D}^{*+}} (m_{\rm B^0} - m_{{\rm D}^{*+}})^2 {\rm K}(\omega)(\omega^2-1)^{1/2} \mathcal{F}^2_{{\rm D}^{*+}}(\omega) |V_{\rm cb}|^2 \;, \qquad (1)$$

where ω, the scalar product of the two meson four-velocities, is related to q^2, the mass squared of the $\ell\nu_\ell$ system: $\omega = (m^2_{\rm B^0} + m^2_{{\rm D}^{(*)+}} - q^2)/(2 m_{\rm B^0} m_{{\rm D}^{(*)+}})$. ${\rm K}(\omega)$ is a known kinematic function and $\mathcal{F}_{{\rm D}^{*+}}(\omega)$ is the hadronic form factor of the decay $\overline{\rm B}^0 \to {\rm D}^{*+}\ell^-\overline{\nu}_\ell$.

The strategy used [8] is to measure $\mathcal{F}_{{\rm D}^{*+}}(1)|V_{\rm cb}|$ from ${\rm d}\Gamma/{\rm d}\omega$ by extrapolation to $\omega = 1$ (point of zero recoil of the ${\rm D}^{*+}$ meson) and to determine $|V_{\rm cb}|$ using the theoretical prediction of $\mathcal{F}_{{\rm D}^{*+}}(1)$. The theoretical uncertainty in this determination is of order 3% [9].

The semileptonic decay $\overline{\rm B}^0 \to {\rm D}^+\ell^-\overline{\nu}_\ell$ can also be used to measure $|V_{\rm cb}|$, though it is more difficult experimentally. In the limit of zero lepton mass the differential decay rate of $\overline{\rm B}^0 \to {\rm D}^+\ell^-\overline{\nu}_\ell$ is:

$$\frac{{\rm d}\Gamma_{{\rm D}^{+}}}{{\rm d}\omega}(\omega) \;=\; \frac{{\rm G_F^2}}{48\pi^3} m^3_{{\rm D}^{+}} (m_{\rm B^0} + m_{{\rm D}^{+}})^2 (\omega^2-1)^{3/2} \mathcal{F}^2_{{\rm D}^{+}}(\omega) |V_{\rm cb}|^2. \qquad (2)$$

At zero recoil, ${\rm d}\Gamma_{{\rm D}^+}/{\rm d}\omega$ is much more suppressed than ${\rm d}\Gamma_{{\rm D}^{*+}}/{\rm d}\omega$ due to helicity mismatch between initial and final states. The strategy to extract $\mathcal{F}_{{\rm D}^+}(1)|V_{\rm cb}|$ is identical to that used for the decay $\overline{\rm B}^0 \to {\rm D}^{*+}\ell^-\overline{\nu}_\ell$ and the theoretical uncertainty in the determination of $|V_{\rm cb}|$ is of the same order [10].

In this letter an update of a previous measurement [6] of $\mathcal{F}_{{\rm D}^{*+}}(1)|V_{\rm cb}|$ from the decay $\overline{\rm B}^0 \to {\rm D}^{*+}\ell^-\overline{\nu}_\ell$ is presented and a measurement of $\mathcal{F}_{{\rm D}^+}(1)|V_{\rm cb}|$ based on the study of the decay $\overline{\rm B}^0 \to {\rm D}^+\ell^-\overline{\nu}_\ell$ is reported. The new analysis allows a comparison of the form factors $\mathcal{F}_{{\rm D}^{*+}}(\omega)$ and $\mathcal{F}_{{\rm D}^+}(\omega)$ which are predicted to be identical in the infinitely heavy quark limit. The value of the ratio $\mathcal{F}_{{\rm D}^{*+}}(1)/\mathcal{F}_{{\rm D}^+}(1)$ provides an important test of the predictions of HQET. A value of $|V_{\rm cb}|$ is also extracted by combining both decays and using constraints [9] on the slope and curvature of the hadronic form factors $\mathcal{F}_{{\rm D}^{*+}}(\omega)$ and $\mathcal{F}_{{\rm D}^+}(\omega)$.

2 The ALEPH detector

The ALEPH detector and its performance are described in detail in Ref. [11, 12]: only a brief description of the apparatus properties is given in this section. Charged particles are detected in the central part of the detector with three concentric devices, a precision vertex detector (VDET), a multi-wire drift chamber (ITC) and a large time projection chamber (TPC). Surrounding the beam pipe, the VDET consists of two concentric layers of double-sided silicon detectors, positioned at average radii of 6.5 cm and 11.3 cm, and covering 85% and 69% of the solid angle, respectively. The intrinsic spatial resolution of the VDET is 12 μm for the $r\phi$ coordinate and between 11 μm and 22 μm for the z coordinate, depending on the polar angle of the charged particle. The ITC, at radii between 16 cm and 26 cm, provides up to 8 coordinates per track in the $r\phi$ view while the TPC measures up to 21 three-dimensional points per track at radii between 30 cm and 180 cm. The TPC also serves to identify charged particle species with up to 338 measurements of the specific ionization ($\mathrm{d}E/\mathrm{d}x$). The three detectors are immersed in an axial magnetic field of 1.5 T and together provide a transverse momentum resolution of $\sigma(p_T)/p_T = 0.0006 \times p_T \bigoplus 0.005$ (p_T in GeV/c).

Electrons and photons are identified in the electromagnetic calorimeter (ECAL), a lead-proportional chamber sandwich segmented into $0.9^\circ \times 0.9^\circ$ projective towers which are read out in three sections in depth. Muons are identified in the hadron calorimeter (HCAL), a 7 interaction length yoke interleaved with 23 layers of streamer tubes, together with two additional double layers of muon chambers. The visible energy flow in the detector is determined with an algorithm [12] which combines measurements from different detector components.

3 Event selection and reconstruction

The analysis presented in this letter is based on approximately 3.9 million hadronic Z decays recorded with the ALEPH detector from 1991 to 1995 and selected as described in Ref. [13].

Exclusive semileptonic decays $\overline{\mathrm{B}}^0 \to \mathrm{D}^{*+}\ell^-\overline{\nu}_\ell$ and $\overline{\mathrm{B}}^0 \to \mathrm{D}^{+}\ell^-\overline{\nu}_\ell$ are selected in hadronic events where a lepton is associated with a D^{*+} or D^{+}, respectively, in the same hemisphere. Throughout this letter, "lepton" refers to either electron or muon, and charge conjugate reactions are implied.

The lepton identification is described in detail in Ref. [14]. Electrons are identified by their shower shape in the ECAL and, when available, by the specific ionization information from the TPC. Muons are identified from their hit pattern in the HCAL and from the presence of at least one associated hit in the muon chambers. Electrons and muons are required to have momentum greater than 2 GeV/c and 3 GeV/c, respectively.

3.1 $\overline{\mathrm{B}}^0 \to \mathrm{D}^{*+}\ell^-\overline{\nu}_\ell$ event selection

D^{*+} candidates are reconstructed in the channel $\mathrm{D}^{*+} \to \mathrm{D}^0\pi^+$ and the D^0 candidates in the three decay modes: $\mathrm{D}^0 \to \mathrm{K}^-\pi^+$, $\mathrm{D}^0 \to \mathrm{K}^-\pi^+\pi^-\pi^+$ and $\mathrm{D}^0 \to \mathrm{K}^0_{\mathrm{s}}\pi^-\pi^+$. The mass difference between the $\mathrm{D}^0\pi^+$ and the D^0 candidates is required to be within 2.1 MeV/c^2 (2.5 standard deviations) of 145.4 MeV/c^2. The event selection is similar to that described in Ref. [6].

Charged kaon candidates for which $\mathrm{d}E/\mathrm{d}x$ information is available are required to have $|\chi_{\mathrm{K}}| < 2$, where χ_{K} is the number of standard deviations between the measured and the expected ionization for the kaon hypothesis. In the channel $\mathrm{D}^0 \to \mathrm{K}^-\pi^+\pi^-\pi^+$, candidate kaons with momenta less than 2 GeV/c are rejected. Candidate $\mathrm{K}^0_{\mathrm{S}}$'s are reconstructed in the channel $\mathrm{K}^0_{\mathrm{S}} \to \pi^-\pi^+$. They must have a momentum larger than 0.5 GeV/c, a decay length larger than 0.5 cm, and a reconstructed mass within 15 MeV/c^2 of the nominal $\mathrm{K}^0_{\mathrm{S}}$ mass. Reconstructed D^0 candidates are required to have a vertex separated from the interaction point by more than twice the resolution on the D^0 reconstructed decay distance.

Reconstructed D^{*+} candidates are combined with an identified lepton from the same hemisphere. The angle between the D^{*+} and the lepton is required to be less than 45°. The $\mathrm{D}^{*+}\ell^-$ system is required to have an invariant mass less than 5.3 GeV/c^2. To ensure a good B meson vertex reconstruction, the lepton and at least two of the D^0 tracks are required to have one or more VDET hits. The χ^2 probabilities of the vertex fit for both D^0 and $\mathrm{D}^{*+}\ell^-$ vertices[2] must be larger than 1%. To ensure a precise measurement of the B meson direction and consequently a good ω reconstruction, the distance of the $\mathrm{D}^{*+}\ell^-$ vertex from the interaction point projected onto the $\mathrm{D}^{*+}\ell^-$ direction is required to be greater than 1 mm. The selection results in a sample of 1266 $\mathrm{D}^{*+}\ell^-$ candidates with a reconstructed D^0 mass within 2.5 standard deviations (σ = 10 MeV/c^2 for $\mathrm{D}^0 \to \mathrm{K}^-\pi^+$ and $\mathrm{D}^0 \to \mathrm{K}^0_{\mathrm{s}}\pi^-\pi^+$ and 8 MeV/c^2 for $\mathrm{D}^0 \to \mathrm{K}^-\pi^+\pi^-\pi^+$) of the D^0 nominal mass.

3.2 $\overline{\mathrm{B}}^0 \to \mathrm{D}^+\ell^-\overline{\nu}_\ell$ event selection

D^+ candidates are reconstructed in the channel $\mathrm{D}^+ \to \mathrm{K}^-\pi^+\pi^+$. The momenta of the two pions are required to be greater than 1 GeV/c for the energetic pion and greater than 0.5 GeV/c for the other, and candidate kaons are selected as in the $\mathrm{D}^0 \to \mathrm{K}^-\pi^+\pi^-\pi^+$ channel. Reflections from $\mathrm{D}^+_{\mathrm{s}} \to \mathrm{K}^-\mathrm{K}^+\pi^+$ are rejected if the $\mathrm{K}^-\mathrm{K}^+$ mass is within 6 MeV/c^2 of the ϕ meson mass or the $\mathrm{K}^-\pi^+$ mass is within 100 MeV/c^2 of the $\overline{\mathrm{K}}^{*0}$ mass and if the reconstructed $\mathrm{K}^+\mathrm{K}^-\pi^-$ mass is within 20 MeV/c^2 of the nominal $\mathrm{D}^+_{\mathrm{s}}$ mass. Reconstructed D^+ candidates are required to have a vertex separated from the interaction point by more than five times the resolution of the D^+ decay distance.

Reconstructed D^+ candidates are combined with an identified lepton from the same hemisphere using the same selection criteria as in the $\mathrm{D}^{*+}\ell^-$ event selection. An additional requirement is placed on the distance between the D^+ vertex and the $\mathrm{D}^+\ell^-$ vertex projected onto the D^+ direction which is required to be greater

[2]The $\mathrm{D}^{*+}\ell^-$ vertex is determined from the lepton and the D^0 candidates.

than -0.5 mm. The selection results in a sample of 1609 $D^+\ell^-$ candidates with a reconstructed D^+ mass within 2.5 standard deviations ($\sigma = 8$ MeV/c^2) of the D^+ nominal mass.

3.3 ω reconstruction

The reconstruction of the ω variable is performed on an event by event basis using the B meson direction and the neutrino energy [6]. The B meson direction is determined from the vector joining the $D^{(*)+}\ell^-$ vertex and the primary vertex. The resolution is inversely proportional to the decay length, and is approximately one degree at a decay-length of three millimeters. The neutrino energy is estimated with a rms precision of 2.6 GeV from the missing energy in the hemisphere containing the $D^{(*)+}\ell^-$ candidate [15]. The rms resolution in ω is 0.07 for both channels corresponding to 13% of the allowed kinematical ranges, $1 < \omega < 1.504$ for the $\overline{B}^0 \to D^{*+}\ell^-\overline{\nu}_\ell$ channel and $1 < \omega < 1.589$ for the $\overline{B}^0 \to D^+\ell^-\overline{\nu}_\ell$ channel.

4 Sample composition and background rejection

4.1 Background sources

The two main classes of background sources that contribute to the $D^{(*)+}\ell^-$ sample are physics background events where the $D^{(*)+}$ and the lepton candidates are both real and combinatorial background events. Combinatorial background events come from either a fake $D^{(*)+}$ in association with a real or a fake lepton, or a fake lepton in association with a real $D^{(*)+}$.

Physics background processes contributing to the $D^{*+}\ell^-$ and $D^+\ell^-$ samples and their measured or estimated branching ratios are listed in Table 1. Processes involving a D^{*+} meson in the final state contribute[3] to both $D^{*+}\ell^-$ and $D^+\ell^-$ samples while processes involving a D^+ meson contribute to the $D^+\ell^-$ sample only. Some of these processes have not been measured and are estimated from other measurements or by analogy with known decays. The branching ratios of $B^- \to D^{(*)+}\pi^-\ell^-\overline{\nu}_\ell$, $\overline{B}^0 \to D^{(*)+}\pi^0\ell^-\overline{\nu}_\ell$ and $\overline{B_s}^0 \to D^{(*)+}K^0\ell^-\overline{\nu}_\ell$ are estimated from measured values [16] of $Br(B^- \to D^{(*)+}\pi^-\ell^-\overline{\nu}_\ell)$ and $Br(\overline{B}^0 \to D^0\pi^-\ell^-\overline{\nu}_\ell)$, using isospin and flavour SU(3) symmetry. The branching ratios of $\overline{B}^0 \to D^{(*)+}\tau^-\overline{\nu}_\tau$ are estimated from the inclusive measurement $Br(b \to X\tau^-\nu_\tau)$ [17], assuming that three-fourths of $b \to X\tau^-\nu_\tau$ involve a D^{*+} meson and the other one-fourth involve a D^+ meson. The branching ratios of the inclusive double charmed B decays $\overline{B} \to D^{*+}X_c$ and $\overline{B} \to D^+X_c$ are based on measurements [18] of $\overline{B} \to D^{(*)+}\overline{D}X$.

For the $D^{*+}\ell^-$ combinatorial background, fake D^{*+}'s arise from the combination of a fake D^0 with a random slow pion or from the combination of a real D^0 with a random slow pion. The first combination leads to a smooth D^0 mass distribution

[3]The decay process $\overline{B}^0 \to D^{*+}\ell^-\overline{\nu}_\ell$ is the signal in the $D^{*+}\ell^-$ sample, and the main physics background component in the $D^+\ell^-$ sample. The $Br(\overline{B}^0 \to D^{*+}\ell^-\overline{\nu}_\ell)$ value in Table 1 is the one measured from the $D^{*+}\ell^-$ sample (see section 5.1).

Table 1: Branching fraction of physics background processes used in this analysis.

Channels contributing to $D^{*+}\ell^-$ and $D^+\ell^-$	Branching fraction (%)	Channels contributing to $D^+\ell^-$	Branching fraction (%)
$B^- \to D^{*+}\pi^-\ell^-\overline{\nu}_\ell$	1.25 ± 0.22	$B^- \to D^+\pi^-\ell^-\overline{\nu}_\ell$	0.32 ± 0.22
$\overline{B}^0 \to D^{*+}\pi^0\ell^-\overline{\nu}_\ell$	0.63 ± 0.11	$\overline{B}^0 \to D^+\pi^0\ell^-\overline{\nu}_\ell$	0.16 ± 0.11
$\overline{B_s}^0 \to D^{*+}K^0\ell^-\overline{\nu}_\ell$	1.25 ± 0.22	$\overline{B_s}^0 \to D^+K^0\ell^-\overline{\nu}_\ell$	0.32 ± 0.22
$\overline{B}^0 \to D^{*+}\tau^-\overline{\nu}_\tau$	2.06 ± 0.41	$\overline{B}^0 \to D^+\tau^-\overline{\nu}_\tau$	0.69 ± 0.14
$\overline{B} \to D^{*+}X_c$	13.0 ± 3.70	$\overline{B} \to D^+X_c$	4.00 ± 3.30
		$\overline{B}^0 \to D^{*+}\ell^-\overline{\nu}_\ell$	5.53 ± 0.58

under the D^0 mass peak in the $D^{*+}\ell^-$ sample. It is fitted with a second order polynomial function and its rate is estimated from the integral of the fitted function within the D^0 mass window. The rate of the second type of combination is estimated by assuming that the probability to associate a random soft pion to a genuine $D^0\ell^-$ pair is the same as to associate a second soft pion to a reconstructed $D^{*+}\ell^-$ combination. This leads to a contribution of less than 1% of the signal at 95% confidence level. The fake lepton combinatorial background is estimated by applying a 1% probability of hadron misidentification (based on Ref. [14]) to D^{*+}-hadron combinations selected with the same criteria as $D^{*+}\ell^-$ combinations.

The $D^+\ell^-$ combinatorial background is estimated in a similar way. In addition, reflections from $D_s^+ \to K^-K^+\pi^+$ are reduced to less than 2% of the signal, as estimated from Monte Carlo, with specific cuts as described in Section 3. Reflections from $\Lambda_c^+ \to pK^-\pi^+$ and $D^{*+} \to D^0(\to K^-\pi^+X)\pi^+$ are negligible.

4.2 Background rejection

The expected composition of the $D^{*+}\ell^-$ and $D^+\ell^-$ samples after event selection is presented in Table 2. The background level is clearly high especially in the $D^+\ell^-$ sample: the fraction of $D^{*+}\ell^-$ ($D^+\ell^-$) events originating from physics background processes is 28% (32%) and from combinatorial background is 16% (42%).

Table 2: The $D^{(*)+}\ell^-$ samples composition without (initial) and with (final) background rejection requirements.

	$D^{*+}\ell^-$ sample		$D^+\ell^-$ sample	
Sample composition	Initial	Final	Initial	Final
Yield	1266 ± 36	741 ± 27	1562 ± 40	466 ± 23
$\overline{B}^0 \to D^{*+}\ell^-\overline{\nu}_\ell$ ($D^{*+} \to D^+\pi^0$)	-	-	249 ± 26	79 ± 8
$B \to D^{(*)+}X\ell^-\overline{\nu}_\ell$	263 ± 46	74 ± 13	163 ± 53	28 ± 10
$\overline{B} \to D^{(*)+}X_c$	71 ± 20	15 ± 5	50 ± 22	7 ± 4
$\overline{B}^0 \to D^{(*)+}\tau^-\overline{\nu_\tau}$	23 ± 5	5 ± 1	31 ± 6	4 ± 1
Comb. background	204 ± 27	68 ± 9	661 ± 47	85 ± 6
Signal	705 ± 68	579 ± 32	408 ± 88	261 ± 23

To reduce the level of background in the two selected samples, three additional requirements are used. The contribution of the process $B^- \to D^{(*)+}\pi^-\ell^-\overline{\nu}_\ell$ in both samples is reduced by rejecting events where an additional charged particle is consistent with the B vertex. Events with an additional charged track in a 45° cone around the $D^{(*)+}\ell^-$ direction, having the same charge as the lepton, momentum greater than 0.5 GeV/c, one or more VDET hits in $r\phi$ and z coordinates, and forming an invariant mass with the $D^{(*)+}\ell^-$ system lower than 5.3 GeV/c^2 are selected. They are rejected if the charged track passes closer to the B vertex than to the interaction point and if its impact parameter with respect to the B vertex is less than 4σ. This requirement removes 77% of the $B^- \to D^{(*)+}\pi^-\ell^-\overline{\nu}_\ell$ background while keeping 96% of the signal. For the channels $D^+ \to K^-\pi^+\pi^+$ and $D^0 \to K^-\pi^+\pi^-\pi^+$, events with an additional track having a charge opposite to that of the lepton and satisfying the same criteria as described above but with the impact parameter calculated with respect to the D vertex instead of the B vertex, are rejected. This requirement removes 30% of the remaining combinatorial background while keeping 99% of the signal.

To reject background $D^{(*)+}\ell^-$ events with additional neutral particles originating from B decay, a missing mass variable $M^2_{\rm miss}$ quantifying the consistency between the neutrino energy, the B direction of flight, the B mass and the $D^{(*)+}\ell^-$ four-momentum is used as described in Ref. [6]. Candidates with $M^2_{\rm miss}$ greater than 1 GeV$^2/c^4$ are rejected. This requirement removes 49% of the $\overline{B} \to D^{(*)+}\pi^0/K^0\ell^-\overline{\nu}_\ell$ while keeping 83% of the signal.

The contribution of background processes $\overline{B}^0 \to D^{*+}\ell^-\overline{\nu}_\ell$, $D^{*+} \to D^+\pi^0/\gamma$ (referred to hereafter as $D^+\pi^0_*\ell^-$) to the $D^+\ell^-$ sample can be further reduced by rejecting $D^+\ell^-$ pairs correlated with a π^0 or a γ. Since $Br(D^{*+} \to D^+\gamma)$ is small compared to $Br(D^{*+} \to D^+\pi^0)$ [19], only π^0 are considered. Due to the soft π^0_* momentum, no explicit reconstruction of the π^0_* is attempted. Photons with energy greater than 500 MeV are selected in a 45° cone around the D^+ direction. A mass difference variable is defined as $\Delta M_\gamma = M(D^+\gamma) - (M_{D^{*+}} + M_{D^+})/2$, which is expected to be close to zero for photons coming from $D^+\pi^0_*\ell^-$. Events where at least one photon fulfills $|\Delta M_\gamma| < 20$ MeV/c^2 are rejected. This requirement removes 54% of the $D^+\pi^0_*\ell^-$ background while keeping 83% of the $D^+\ell^-$ signal. Fig. 1 shows the mass difference ΔM_γ for signal and background events estimated as described in section 4.1.

The expected compositions of the $D^{*+}\ell^-$ and $D^+\ell^-$ samples after background rejection requirements are described in Table 2. The contribution of physics and combinatorial background events in the final $D^{(*)+}\ell^-$ sample have been strongly reduced. The expected fraction of physics background $D^{*+}\ell^-$ ($D^+\ell^-$) events is 13% (25%). The expected fraction of combinatorial background $D^{*+}\ell^-$ ($D^+\ell^-$) events is 9% (18%). The reconstructed ω distributions of the final $D^{*+}\ell^-$ and $D^+\ell^-$ samples are presented in Fig. 2 along with the main background contributions.

The reconstruction efficiencies for $\overline{B}^0 \to D^{*+}\ell^-\overline{\nu}_\ell$ and $\overline{B}^0 \to D^+\ell^-\overline{\nu}_\ell$ decays are estimated from Monte Carlo simulation. Differences in efficiency of the VDET hits and vertices probability requirements between data and Monte Carlo are investigated in detail on inclusive D^{*+}, D^+, $D^{*+}\ell^-$ and $D^+\ell^-$ samples and corrections are applied to the simulation efficiencies [6]. The variation of the reconstruction efficiencies as a function of ω for all reconstructed decay channels is presented in Fig. 3.

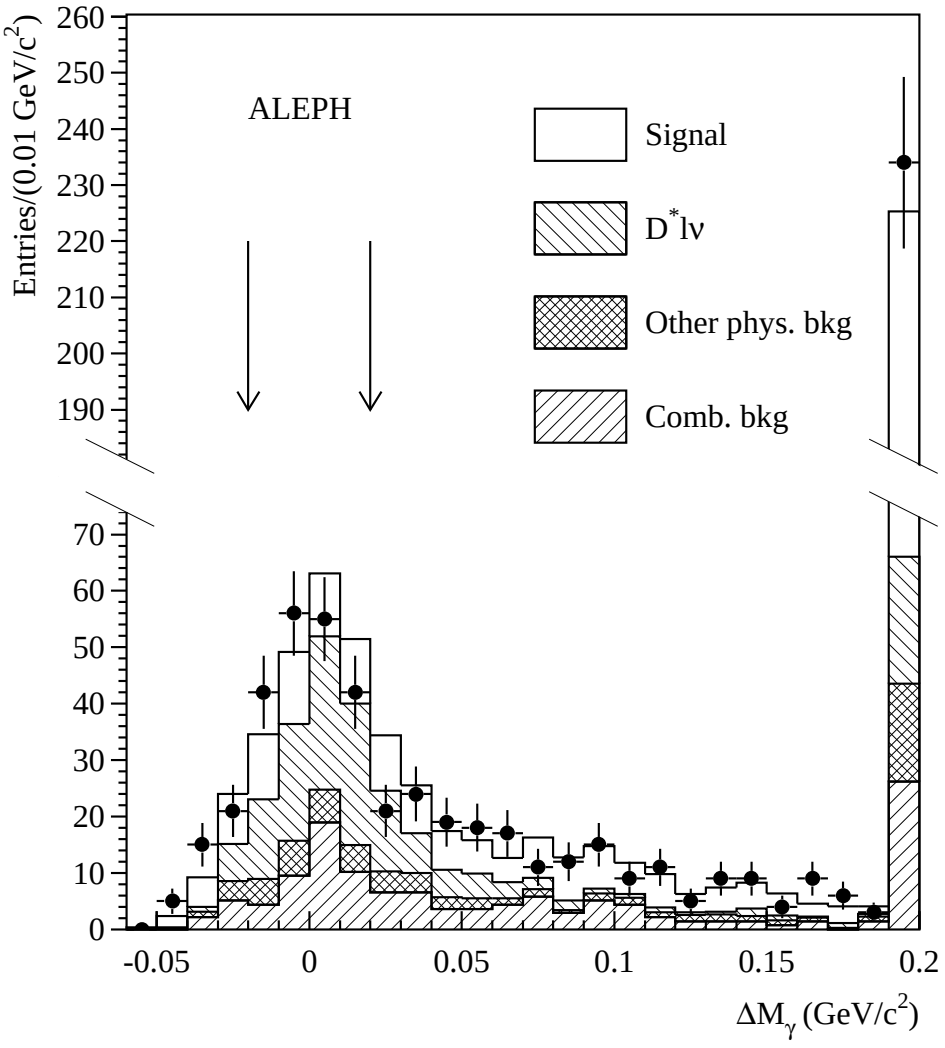

Figure 1: The reconstructed ΔM_γ for data (points), and backgrounds (histograms). If several photons are available, the one with ΔM_γ closest to zero is selected. The arrows indicate the excluded region. The rightmost bin contains overflows and events with no photon candidate. The vertical scale is broken for better readability.

5 Measurement of $\mathcal{F}_{\mathrm{D}^{*+}}(1)|V_{\mathrm{cb}}|$ and $\mathcal{F}_{\mathrm{D}^{+}}(1)|V_{\mathrm{cb}}|$

The method used to extract $\mathcal{F}_{\mathrm{D}^{*+}}(1)|V_{\mathrm{cb}}|$ and $\mathcal{F}_{\mathrm{D}^{+}}(1)|V_{\mathrm{cb}}|$ from the differential event rate $\mathrm{d}N(\mathrm{D}^{*+}\ell^-)/\mathrm{d}\omega$ and $\mathrm{d}N(\mathrm{D}^{+}\ell^-)/\mathrm{d}\omega$ is described in this section. The systematic error quoted for each result is described in the next section.

5.1 Measurement of $\mathcal{F}_{\mathrm{D}^{*+}}(1)|V_{\mathrm{cb}}|$

The combinatorial background contribution to $\mathrm{d}N(\mathrm{D}^{*+}\ell^-)/\mathrm{d}\omega$ is measured from data in each bin of ω as described in Section 4.1 while physics background contributions are taken from dedicated Monte Carlo simulation, with total number of events

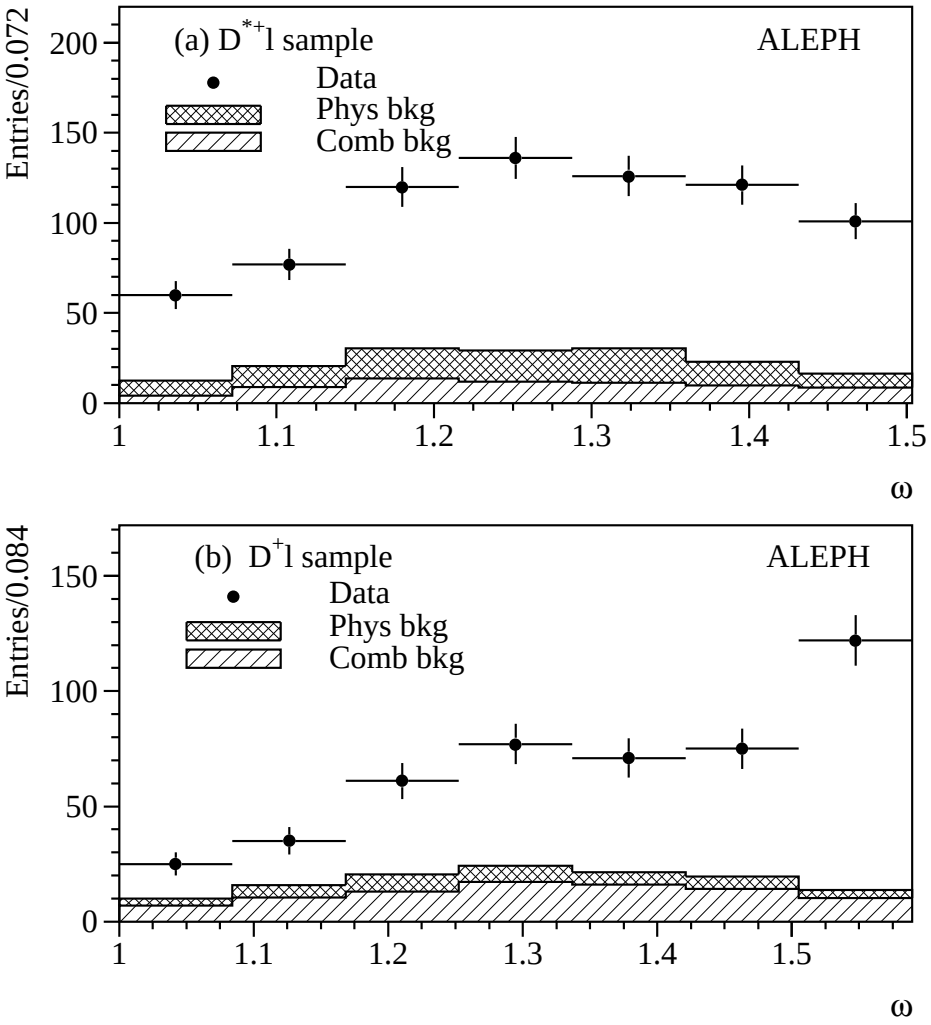

Figure 2: Reconstructed ω distributions for (a) $\overline{\mathrm{B}}^0 \to \mathrm{D}^{*+}\ell^-\overline{\nu}_\ell$ and (b) $\overline{\mathrm{B}}^0 \to \mathrm{D}^{+}\ell^-\overline{\nu}_\ell$ event candidates. The points are data. The black histograms are the combinatorial background contributions. The shaded histograms correspond to the various physics backgrounds reconstructed from dedicated Monte Carlo. The $\mathrm{D}^+\pi^0_*\ell^-$ contribution in (b) is not shown, since it is to be measured from data (see section 5.2).

as given in Table 2.

The physics function which describes the $\mathrm{d}N(\mathrm{D}^{*+}\ell^-)/\mathrm{d}\omega$ distribution of the final $\overline{\mathrm{B}}^0 \to \mathrm{D}^{*+}\ell^-\overline{\nu}_\ell$ sample after background subtraction is

$$\Phi(\omega) = 2\frac{N_{\mathrm{q\bar{q}}}}{\epsilon_{\mathrm{q\bar{q}}}}\frac{\Gamma_{\mathrm{b\bar{b}}}}{\Gamma_{\mathrm{had}}}\mathrm{Br}(\mathrm{b}\to \mathrm{B}^0)\mathrm{Br}(\mathrm{D}^{*+}\to \mathrm{D}^0\pi^+)\mathrm{Br}(\mathrm{D}^0\to \mathrm{K}n\pi)\frac{\tau_{\mathrm{B}^0}}{\hbar}\frac{\mathrm{d}\Gamma_{\mathrm{D}^{*+}}(\omega)}{\mathrm{d}\omega}\epsilon(\omega)\ ,$$

where $\mathrm{Br}(\mathrm{D}^0\to \mathrm{K}n\pi)$ is the branching ratio of the D^0 decay. Its value for the three decay channels is given in Table 3. The quantity $\epsilon_{\mathrm{q\bar{q}}} = 97.40 \pm 0.24\%$ [13] is the hadronic event selection efficiency and $\epsilon(\omega)$ is the ω-dependent selection efficiency.

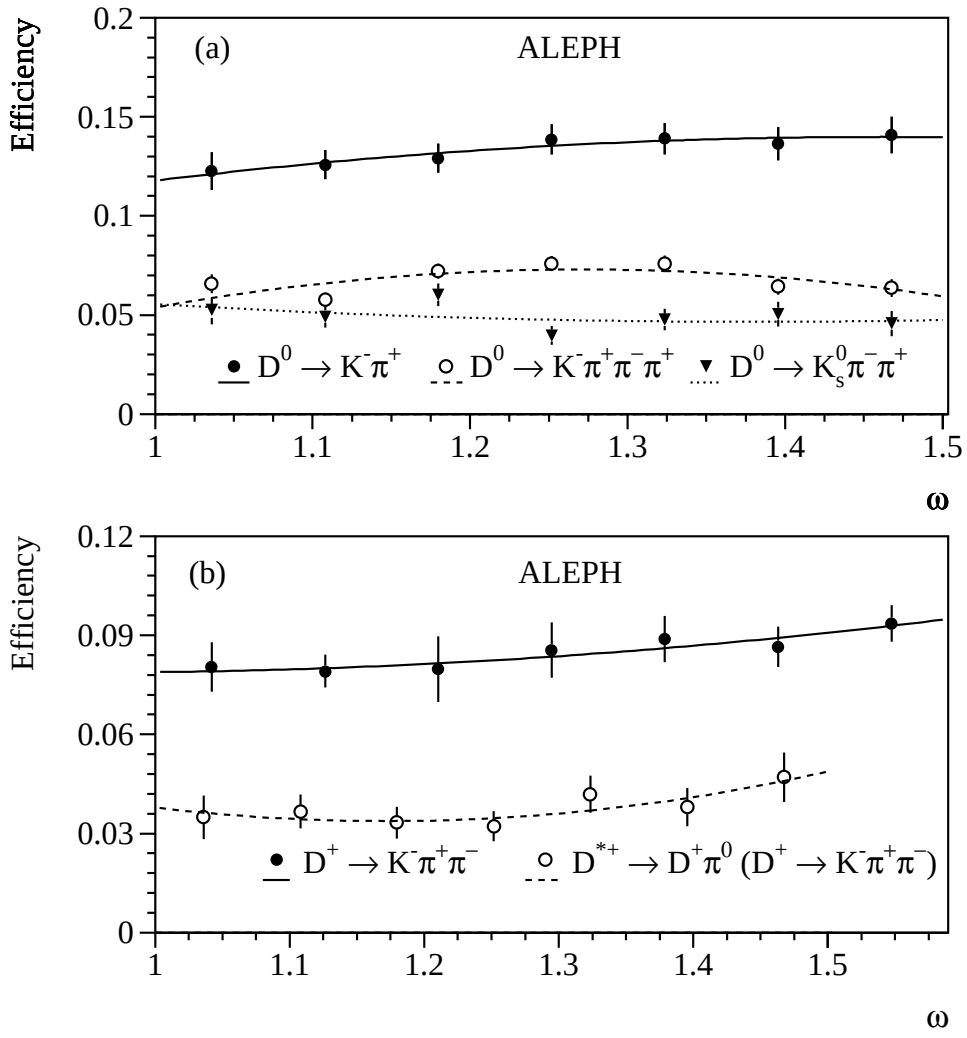

Figure 3: Reconstruction efficiency for (a) $\overline{\mathrm{B}}^0 \to \mathrm{D}^{*+}\ell^-\overline{\nu}_\ell$ decay and (b) $\overline{\mathrm{B}}^0 \to \mathrm{D}^+(\pi^0_*)\ell^-\overline{\nu}_\ell$ decay as a function of ω. The curves are the second order polynomial fits used to parameterize the efficiency in the fit.

The latter is parameterized for each D^0 decay channel by a second order polynomial. The differential decay width $\mathrm{d}\Gamma_{\mathrm{D}^{*+}}/\mathrm{d}\omega$ is given in Eq. 1.

The unknowns in the physics function $\Phi(\omega)$ are $|V_{\mathrm{cb}}|$ and $\mathcal{F}_{\mathrm{D}^{*+}}(\omega)$. The dependence of $\mathcal{F}_{\mathrm{D}^{*+}}(\omega)$ on ω is assumed to be linear:

$$\mathcal{F}_{\mathrm{D}^{*+}}(\omega) = \mathcal{F}_{\mathrm{D}^{*+}}(1)[1 - a^2_{\mathrm{D}^{*+}}(\omega - 1)] \; .$$

A binned maximum likelihood fit is performed on the $\mathrm{d}N(\mathrm{D}^{*+}\ell^-)/\mathrm{d}\omega$ distribution. The fitting function is the convolution of the physics function $\Phi(\omega)$ and the ω-dependent resolution function.

The results are given in Table 4. Fig. 4a shows the result of the fit. The corresponding product $\mathcal{F}_{\mathrm{D}^{*+}}(\omega)|V_{\mathrm{cb}}|$ is shown in Fig. 4b. The values of $\mathcal{F}_{\mathrm{D}^{*+}}(\omega)|V_{\mathrm{cb}}|$

Table 3: Branching fractions and lifetimes used [19]. The quoted errors are used for the estimation of systematic uncertainties.

	Branching fractions (%)
$\Gamma_{b\bar{b}}/\Gamma_{had}$	22.12 ± 0.20
$Br(b \to B^0)$	37.8 ± 2.2
$Br(b \to B_s^0)$	11.2 ± 1.9
$Br(D^{*+} \to D^0\pi^+)$	68.3 ± 1.4
$Br(D^{*+} \to D^+\pi^0)$	30.6 ± 2.5
$Br(D^{*+} \to D^+\gamma)$	$1.1^{+2.1}_{-0.7}$
$Br(D^0 \to K^-\pi^+)$	3.83 ± 0.12
$Br(D^0 \to K^-\pi^+\pi^-\pi^+)$	7.5 ± 0.4
$Br(D^0 \to K_s^0\pi^-\pi^+)$	2.7 ± 0.2
$Br(D^+ \to K^-\pi^+\pi^+)$	9.1 ± 0.6
	Lifetimes (ps)
τ_{B^0}	1.56 ± 0.06
τ_{B^+}	1.62 ± 0.06
$\tau_{B_s^0}$	1.61 ± 0.10

for specific values of q^2 are useful for tests of the factorization in hadronic decays; they are given in Table 5.

From the integrated physics function, the branching ratio of $\overline{B}^0 \to D^{*+}\ell^-\overline{\nu}_\ell$ is measured to be

$$Br(\overline{B}^0 \to D^{*+}\ell^-\overline{\nu}_\ell) = (5.53 \pm 0.26_{stat} \pm 0.52_{syst})\% \ .$$

5.2 Measurement of $\mathcal{F}_{D^+}(1)|V_{cb}|$

All background contributions to $dN(D^+\ell^-)/d\omega$ are estimated as described in the previous section except for the $D^{*+}\ell^-$ component corresponding to the partially reconstructed $D^+\pi_*^0\ell^-$ decay. The value of $\mathcal{F}_{D^+}(1)|V_{cb}|$ is extracted by fitting simultaneously the $dN(D^+\ell^-)/d\omega$ and $dN(D^{*+}\ell^-)/d\omega$ distributions so that the $D^+\pi_*^0\ell^-$ background component in $dN(D^+\ell^-)/d\omega$ is determined from data.

Table 4: Results of the different fits described in the text. The systematic errors are described in Section 6.

Channel	$\mathcal{F}_{D^{(*)+}}(1)\lvert V_{cb}\rvert(\times 10^{-3})$	$a^2_{D^{(*)+}}$	Correlation
	Linear fit		
$D^{*+}\ell$	$31.9 \pm 1.8_{stat} \pm 1.9_{syst}$	$0.31 \pm 0.17_{stat} \pm 0.08_{syst}$	92%
$D^+\ell$	$27.8 \pm 6.8_{stat} \pm 6.5_{syst}$	$-0.05 \pm 0.53_{stat} \pm 0.38_{syst}$	99%
	Quadratic constrained fit		
$D^{*+}\ell$	$32.0 \pm 2.1_{stat} \pm 2.0_{syst}$	$0.37 \pm 0.26_{stat} \pm 0.14_{syst}$	94%
$D^+\ell$	$31.1 \pm 9.9_{stat} \pm 8.6_{syst}$	$0.20 \pm 0.98_{stat} \pm 0.50_{syst}$	99%

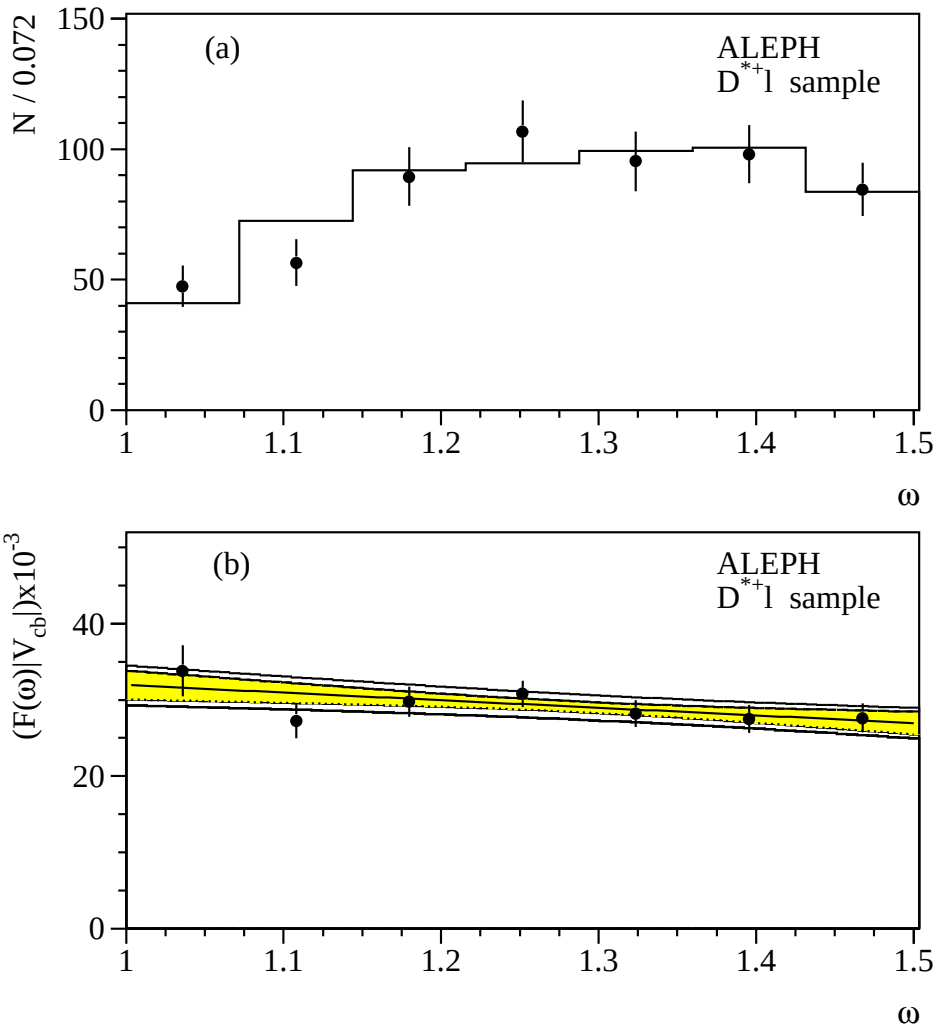

Figure 4: (a) The differential rate $\mathrm{d}N(\mathrm{D}^{*+}\ell^-)/\mathrm{d}\omega$ of $\overline{\mathrm{B}}^0 \to \mathrm{D}^{*+}\ell^-\overline{\nu}_\ell$ candidates after all cuts and background subtraction. The points are data with statistical error bars, and the histogram is the number of events predicted by the fit. (b) $\mathcal{F}_{\mathrm{D}^{*+}}(\omega)|V_{\mathrm{cb}}|$ as a function of ω, the shaded band and the white bands indicating the statistical and systematic uncertainties, respectively. The points are data after correction for resolution effects.

The physics function describing the $\mathrm{d}N(\mathrm{D}^+\ell^-)/\mathrm{d}\omega$ distribution after subtracting all backgrounds except the remaining $\mathrm{D}^+\pi^0_*\ell^-$ component is:

$$\begin{aligned}\Phi(\omega) &= 2\frac{N_{\mathrm{q\bar{q}}}}{\epsilon_{\mathrm{q\bar{q}}}}\frac{\Gamma_{\mathrm{b\bar{b}}}}{\Gamma_{\mathrm{had}}}\mathrm{Br}(\mathrm{b}\to \mathrm{B}^0)\mathrm{Br}(\mathrm{D}^+\to \mathrm{K}^-\pi^+\pi^+)\frac{\tau_{\mathrm{B}^0}}{\hbar} \\ &\times \left[\frac{\mathrm{d}\Gamma_{\mathrm{D}^+}}{\mathrm{d}\omega}(\omega)\epsilon_{\mathrm{D}^+}(\omega) + \mathrm{Br}(\mathrm{D}^{*+}\to \mathrm{D}^+\pi^0/\gamma)\frac{\mathrm{d}\Gamma_{\mathrm{D}^{*+}}}{\mathrm{d}\omega}(\omega)\epsilon_{\mathrm{D}^{*+}}(\omega)\right] .\end{aligned}$$

The ω-dependent selection efficiencies $\epsilon_{\mathrm{D}^+}(\omega)$ for the $\overline{\mathrm{B}}^0 \to \mathrm{D}^+\ell^-\overline{\nu}_\ell$ signal and $\epsilon_{\mathrm{D}^{*+}}(\omega)$ for the $\overline{\mathrm{B}}^0 \to \mathrm{D}^{*+}\ell^-\overline{\nu}_\ell$ background are both parameterized by second order polyno-

Table 5: Values of $\mathcal{F}_{\mathrm{D}^+}(\omega)|V_{\mathrm{cb}}|$ and $\mathcal{F}_{\mathrm{D}^{*+}}(\omega)|V_{\mathrm{cb}}|$ for q^2 corresponding to the masses of some particles (note that the same q^2 corresponds to different ω depending on the decay), extracted from the results of the linear fit given in Table 4. The values are also given for the maximum ω. The first uncertainties are statistical and the second are systematic. The entries are largely correlated.

	$\mathcal{F}_{\mathrm{D}^{*+}}(\omega)\|V_{\mathrm{cb}}\|(\times 10^{-3})$	$\mathcal{F}_{\mathrm{D}^+}(\omega)\|V_{\mathrm{cb}}\|\ (\times 10^{-3})$
$\omega = 1$	$31.9 \pm 1.8 \pm 1.9$	$27.8 \pm 6.8 \pm 6.5$
$\omega(m_{\mathrm{D}_s^+})$	$28.0 \pm 0.9 \pm 1.5$	$28.2 \pm 2.3 \pm 3.6$
$\omega(m_{a_1^+})$	$27.6 \pm 1.1 \pm 1.5$	$28.5 \pm 1.2 \pm 2.6$
$\omega(m_{\rho^+})$	$27.2 \pm 1.3 \pm 1.4$	$28.5 \pm 1.6 \pm 2.5$
$\omega(m_{\pi^+})$	$26.9 \pm 1.4 \pm 1.4$	$28.6 \pm 2.0 \pm 2.5$
$\omega_{\mathrm{D}^{*+}}^{\mathrm{max}}$	$26.9 \pm 1.4 \pm 1.4$	$28.4 \pm 1.1 \pm 2.6$
$\omega_{\mathrm{D}^+}^{\mathrm{max}}$	-	$28.6 \pm 2.1 \pm 2.0$

mials. The differential decay widths $\mathrm{d}\Gamma_{\mathrm{D}^{*+}}/\mathrm{d}\omega$ and $\mathrm{d}\Gamma_{\mathrm{D}^+}/\mathrm{d}\omega$ are given in Eqs. 1 and 2, respectively. The form factor $\mathcal{F}_{\mathrm{D}^+}(\omega)$ in $\mathrm{d}\Gamma_{\mathrm{D}^+}/\mathrm{d}\omega$ is assumed to have a linear dependence on ω, as for $\mathcal{F}_{\mathrm{D}^{*+}}(\omega)$ in $\mathrm{d}\Gamma_{\mathrm{D}^{*+}}/\mathrm{d}\omega$:

$$\mathcal{F}_{\mathrm{D}^+}(\omega) = \mathcal{F}_{\mathrm{D}^+}(1)[1 - a^2_{\mathrm{D}^+}(\omega - 1)] \ .$$

A binned maximum likelihood fit is simultaneously performed on the $\mathrm{d}N(\mathrm{D}^+\ell^-)/\mathrm{d}\omega$ and $\mathrm{d}N(\mathrm{D}^{*+}\ell^-)/\mathrm{d}\omega$ distributions. The signal and background components of the $\mathrm{d}N(\mathrm{D}^+\ell^-)/\mathrm{d}\omega$ distribution are convolved with different ω-resolution functions. The ω-resolution function for background $\mathrm{D}^+\pi^0_*\ell^-$ events is worsened due to the missing π^0. The four free parameters in the fit are $\mathcal{F}_{\mathrm{D}^+}(1)|V_{\mathrm{cb}}|$, $a^2_{\mathrm{D}^+}$, $\mathcal{F}_{\mathrm{D}^{*+}}(1)|V_{\mathrm{cb}}|$, and $a^2_{\mathrm{D}^{*+}}$. The results for $\mathcal{F}_{\mathrm{D}^+}(1)|V_{\mathrm{cb}}|$ and $a^2_{\mathrm{D}^+}$ are given in Table 4. Their statistical uncertainties include by construction the uncertainty on the $\mathrm{D}^{*+}\ell^-$ contribution. Values of $\mathcal{F}_{\mathrm{D}^{*+}}(1)|V_{\mathrm{cb}}|$ and $a^2_{\mathrm{D}^{*+}}$ obtained from this simultaneous fit are indistinguishable from those obtained from the previous fit (see Section 5.1) of the $\mathrm{d}N(\mathrm{D}^{*+}\ell^-)/\mathrm{d}\omega$ distribution alone. Fig. 5a shows the result of the fit. The corresponding product $\mathcal{F}_{\mathrm{D}^+}(\omega)|V_{\mathrm{cb}}|$ is shown in Fig. 5b. Values of $\mathcal{F}_{\mathrm{D}^+}(\omega)|V_{\mathrm{cb}}|$ for specific values of the q^2 are also given in Table 5.

From the integrated physics function $\Phi_{\mathrm{D}^+}(\omega)$, the branching ratio of $\overline{\mathrm{B}}^0 \to \mathrm{D}^+\ell^-\overline{\nu}_\ell$ is measured to be

$$\mathrm{Br}(\overline{\mathrm{B}}^0 \to \mathrm{D}^+\ell^-\overline{\nu}_\ell) = (2.35 \pm 0.20_{\mathrm{stat}} \pm 0.44_{\mathrm{syst}})\% \ .$$

5.3 Measurement of $\mathcal{F}_{\mathrm{D}^+}(1)/\mathcal{F}_{\mathrm{D}^{*+}}(1)$ and $|V_{\mathrm{cb}}|$

Fig. 6 shows that the ratio of $\mathcal{F}_{\mathrm{D}^+}(\omega)$ and $\mathcal{F}_{\mathrm{D}^{*+}}(\omega)$ is consistent with unity over the whole common range of ω. At $\omega = 1$ this ratio is measured from the results of the previous fits to be

$$\mathcal{F}_{\mathrm{D}^+}(1)/\mathcal{F}_{\mathrm{D}^{*+}}(1) \ = \ 0.87 \pm 0.22_{\mathrm{stat}} \pm 0.21_{\mathrm{syst}},$$

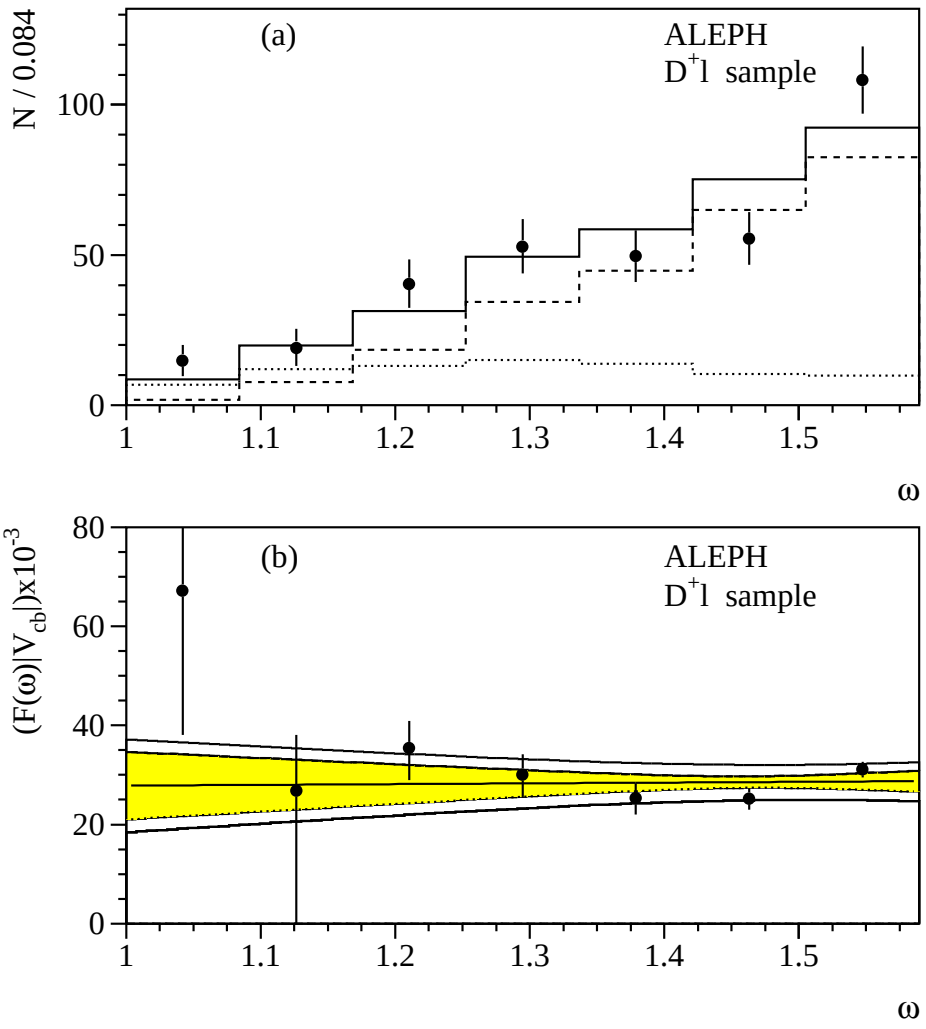

Figure 5: (a) The differential event rate $\mathrm{d}N(\mathrm{D}^+\ell^-)/\mathrm{d}\omega$ of $\overline{\mathrm{B}}^0 \to \mathrm{D}^+\ell^-\overline{\nu}_\ell$ candidates after all cuts and background subtraction. The points are data with statistical error bars. The dotted histogram is the contribution of the $\mathrm{D}^0\pi_*^+\ell^-$ background, the dashed histogram is the contribution of the $\overline{\mathrm{B}}^0 \to \mathrm{D}^+\ell^-\overline{\nu}_\ell$ signal and the solid histogram the sum of the two. (b) $\mathcal{F}_{\mathrm{D}^+}(\omega)|V_{\mathrm{cb}}|$ as a function of ω (see caption of Fig. 4 for details).

in agreement with the theoretical prediction [10] $\mathcal{F}^{\mathrm{th}}_{\mathrm{D}^+}(1)/\mathcal{F}^{\mathrm{th}}_{\mathrm{D}^{*+}}(1) = 1.08 \pm 0.06_{\mathrm{th}}$.

The same quantity is also measured to be consistent with unity with better accuracy at $\omega^{\mathrm{max}}_{\mathrm{D}^{*+}}$, the maximum value of ω for the $\overline{\mathrm{B}}^0 \to \mathrm{D}^{*+}\ell^-\overline{\nu}_\ell$ decay,

$$\mathcal{F}_{\mathrm{D}^+}(\omega^{\mathrm{max}}_{\mathrm{D}^{*+}})/\mathcal{F}_{\mathrm{D}^{*+}}(\omega^{\mathrm{max}}_{\mathrm{D}^{*+}}) \;=\; 1.06 \pm 0.09_{\mathrm{stat}} \pm 0.09_{\mathrm{syst}}.$$

The independence of $\mathcal{F}_{\mathrm{D}^+}(\omega)/\mathcal{F}_{\mathrm{D}^{*+}}(\omega)$ over the whole range of ω is also quantified by verifying that the difference of the fitted slopes is in agreement with the theoretical value [9] $(a^2_{\mathrm{D}^+} - a^2_{\mathrm{D}^{*+}})_{\mathrm{th}} \simeq 0.08$,

$$a^2_{\mathrm{D}^+} - a^2_{\mathrm{D}^{*+}} \;=\; -0.36 \pm 0.58_{\mathrm{stat}} \pm 0.31_{\mathrm{syst}}.$$

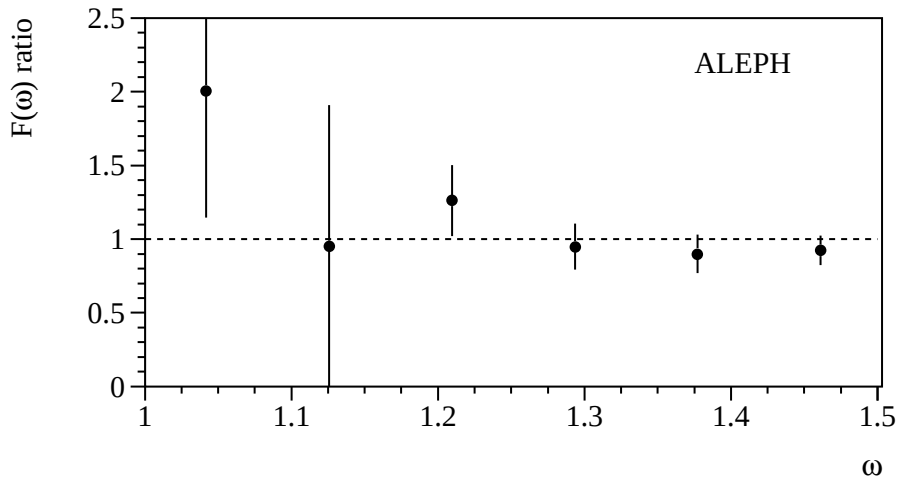

Figure 6: The measured ratio of $\mathcal{F}_{\mathrm{D}^+}(\omega)$ and $\mathcal{F}_{\mathrm{D}^{*+}}(\omega)$, with statistical error bars.

These are the first direct tests of the prediction of HQET that the same hadronic form factor can describe the decays $\overline{\mathrm{B}}^0 \to \mathrm{D}^{*+}\ell^-\overline{\nu}_\ell$ and $\overline{\mathrm{B}}^0 \to \mathrm{D}^{+}\ell^-\overline{\nu}_\ell$. This prediction can be exploited to extract $|V_{\mathrm{cb}}|$ from the two decays, by using the Isgur-Wise function $\mathcal{F}_0(\omega)$ itself. A second-order parameterization

$$\mathcal{F}_0(\omega) = 1 - a_0^2(\omega - 1) + c_0(\omega - 1)^2$$

is chosen and a theoretical constraint [9] $c_0 \simeq 0.72a_0^2 - 0.09$ is used. The form factors $\mathcal{F}_{\mathrm{D}^{*+}}(\omega)$ and $\mathcal{F}_{\mathrm{D}^{+}}(\omega)$ are parameterized similarly, with slopes and curvatures related to those of $\mathcal{F}_0(\omega)$ by the relations [9] $a^2_{\mathrm{D}^{*+}} = a_0^2 - 0.06$, $a^2_{\mathrm{D}^{+}} = a_0^2 + 0.02$, $c_{\mathrm{D}^{*+}} = c_0 - 0.06 - 0.06a_0^2$, $c_{\mathrm{D}^{+}} = c_0 + 0.01 + 0.02a_0^2$. These relations allow the constraint between a_0^2 and c_0 to be transformed into constraints between $a^2_{\mathrm{D}^{(*)+}}$ and $c_{\mathrm{D}^{(*)+}}$. The results are given in Table 4. In spite of the increased uncertainty, this result is chosen since it relies on a less arbitrary parameterization of the form factors [9].

The measurement of $|V_{\mathrm{cb}}|$ is done by fitting directly the Isgur-Wise function with the parameterization given above and taking the normalizations at $\omega = 1$ to be $\mathcal{F}^{\mathrm{th}}_{\mathrm{D}^{*+}}(1) = 0.91 \pm 0.03_{\mathrm{th}}$ (see Ref. [9] and references therein) and $\mathcal{F}^{\mathrm{th}}_{\mathrm{D}^{+}}(1)/\mathcal{F}^{\mathrm{th}}_{\mathrm{D}^{*+}}(1) = 1.08 \pm 0.06_{\mathrm{th}}$. The fitted values of the two remaining free parameters, which are 95% correlated, are:

$$\begin{aligned} |V_{\mathrm{cb}}| &= (34.4 \pm 1.6_{\mathrm{stat}} \pm 2.3_{\mathrm{syst}} \pm 1.4_{\mathrm{th}}) \times 10^{-3} \,, \\ a_0^2 &= 0.30 \pm 0.12_{\mathrm{stat}} \pm 0.14_{\mathrm{syst}} \pm 0.13_{\mathrm{th}} \,, \end{aligned}$$

where the third error arises from the theoretical uncertainty on the inputs.

Table 6: Systematic uncertainties. All contributions are given in percent with respect to the measured value except for $a^2_{\mathrm{D}^+}$ and $a^2_{\mathrm{D}^{*+}}$, where absolute uncertainties are quoted.

Source	$\mathcal{F}_{\mathrm{D}^{*+}}(1)\lvert V_{\mathrm{cb}}\rvert$	$a^2_{\mathrm{D}^{*+}}$	$\mathrm{Br}_{\mathrm{D}^{*+}}$	$\mathcal{F}_{\mathrm{D}^{+}}(1)\lvert V_{\mathrm{cb}}\rvert$	$a^2_{\mathrm{D}^{+}}$	$\mathrm{Br}_{\mathrm{D}^{+}}$
Branch. ratios						
$\mathrm{Br}(\mathrm{D}\to \mathrm{K}n\pi)$	2.0	-	3.8	10.0	0.13	9.5
$\mathrm{Br}(\mathrm{D}^{*+}\to \mathrm{D}^0\pi^+)$	1.4	-	2.8	6.0	0.11	2.7
$\Gamma_{\mathrm{b\bar{b}}}/\Gamma_{\mathrm{had}}$	0.5	-	0.9	0.5	-	0.9
$\mathrm{Br}(\mathrm{b}\to \mathrm{B}^0)$	2.9	-	5.8	2.9	-	5.8
Subtotal	3.8	-	7.5	12.0	0.17	11.5
Background						
$\mathrm{B}^-\to \mathrm{D}^*\mathrm{X}\ell^-\overline{\nu}_\ell$	1.7	0.02	2.2	9.8	0.18	4.3
$\overline{\mathrm{B}}\to \mathrm{D}^{(*)+}\mathrm{X}_{\mathrm{c}}$	0.3	-	0.7	2.3	0.04	1.4
$\overline{\mathrm{B}}^0\to \mathrm{D}^{(*)+}\tau^-\overline{\nu}_\tau$	0.2	-	0.4	1.8	0.04	0.5
Fake $\mathrm{D}^{(*)}$	0.8	-	1.6	2.2	0.01	2.2
Fake lepton	0.7	-	0.4	1.1	0.02	0.5
Subtotal	2.0	0.02	3.5	10.5	0.20	5.1
Simulation						
Fragmentation	1.7	0.02	2.3	3.6	0.03	4.7
ℓ efficiency	1.0	-	2.0	2.0	0.01	2.0
Vertex efficiency	1.5	-	2.9	11.2	0.13	10.5
Photon efficiency	-	-	-	6.0	0.04	6.0
Efficiency shape	0.6	0.02	0.3	4.5	0.10	0.4
MC statistics	1.6	0.05	1.6	8.4	0.19	3.9
ω resolution	1.5	0.05	-	4.7	0.10	-
Subtotal	3.4	0.08	4.5	17.1	0.27	13.7
B^0 **lifetime**	2.6	-	1.5	3.3	0.01	1.4
Total	6.1	0.08	9.5	23.5	0.38	18.6

6 Systematic uncertainties

The various sources of systematic uncertainties are summarized in Table 6. They are described in more detail below. Since $\mathcal{F}(1)|V_{\mathrm{cb}}|$ is proportional to the square root of the branching fraction of the B decay, it will be half as sensitive than the branching fractions to quantities like other branching fractions and efficiencies, provided the slope a^2 is unaffected. This is generally true for the $\mathrm{D}^{*+}\ell^-$ channel, where the signal and the background have similar shapes. For the $\mathrm{D}^+\ell^-$ channel however, the signal vanishes rapidly at low ω, while the background is roughly constant. Any systematic uncertainty affecting the background level will affect both the normalization and the slope, with a comparatively higher impact on $\mathcal{F}(1)|V_{\mathrm{cb}}|$ than for the $\mathrm{D}^{*+}\ell^-$ channel. Correlations between the $\mathrm{D}^{*+}\ell^-$ and the $\mathrm{D}^+\ell^-$ measurements are taken into account in the determination of all uncertainties. The correlation between the total systematic uncertainties on $\mathcal{F}(1)|V_{\mathrm{cb}}|$ and a^2 is 48% for the $\mathrm{D}^{*+}\ell^-$ channel and 93% for the $\mathrm{D}^+\ell^-$ channel. The systematical uncertainty on the ratio $\mathcal{F}_{\mathrm{D}^+}(1)/\mathcal{F}_{\mathrm{D}^{*+}}(1)$ is largely dominated by the uncertainty on $\mathcal{F}_{\mathrm{D}^+}(1)$. The systematical uncertainties

on $|V_{cb}|$ and a_0^2 are similar to the uncertainties on $\mathcal{F}_{D^{*+}}(1)|V_{cb}|$ and $a^2_{D^{*+}}$ but with a larger sensitivity to the background and to the simulation.

Branching fractions: The systematic uncertainties related to the fraction of hadronic Z decays to $b\overline{b}$ pairs and the D^{*+}, D^0 and D^+ branching fractions are estimated by the effect of their variation within the quoted uncertainties in Table 3. Correlations in the measured D^0 branching fractions are taken into account. The branching ratios $Br(D^{*+} \to D^0\pi^+)$ and $Br(D^{*+} \to D^+\pi^0/\gamma)$ are also taken to be fully anti-correlated.

Backgrounds: The contribution of each physics background is varied within uncertainties given in Table 1, taking into account their possible correlation. The fraction of narrow resonant $D^{(*)+}\pi/K\ell^-\overline{\nu}_\ell$ decays in the Monte Carlo simulation is varied between 0 and 100% (with a central value of 46% [16]) to account for the lack of knowledge of the non-resonant part.

The use of a first order polynomial instead of a second order one to describe the fake D background component in the D mass spectrum fit changes the background estimate slightly. The contribution of fake D^{*+} events in the $D^{*+}\ell^-$ sample and of the reflection from $D_s^+ \to K^-K^+\pi^+$ in the $D^+\ell^-$ sample are varied by 100% of their estimated contribution given in Section 4.1. The uncertainty on the fake lepton mis-identification probability (electron or muon) is estimated to be 20%, based on Ref. [14].

Simulation: The mean B hadron energy has been measured by ALEPH to be $x_B = 0.715 \pm 0.015$ [15] relative to the beam energy. The quoted uncertainty corresponds to the variation of the efficiency when x_B is varied within errors. The uncertainty on the lepton efficiency is taken to be 2%, based on Ref. [14].

The data *vs* Monte Carlo efficiency ratio of the VDET hits and vertex probability requirements mentioned in Section 4.2 are varied within errors.

Photon reconstruction affects the selected $D^+\ell^-$ sample in two ways. The efficiency for associating the D^+ with a random photon affects directly the $D^+\ell^-$ efficiency. This effect is checked by comparing in data and Monte Carlo the probability to associate a random photon to $D^0\pi_*^+\ell^-$ events, where no photon is expected. The photon reconstruction efficiency directly affects the level of remaining $D^+\pi_*^0\ell^-$ events. This effect is checked by comparing the number of $D^+\pi_*^0\ell^-$ events passing and failing the photon rejection cut on data and Monte Carlo, as illustrated by the agreement between data and Monte-Carlo in Fig. 1. The quoted uncertainty corresponds to the statistical error of these two successful checks.

The uncertainty related to the ω resolution is taken to be half of the change in parameters when the fit is performed with a perfect resolution. Degrading the ω resolution by arbitrarily shifting the missing energy or smearing the vertices inside their estimated uncertainty or by not using the soft pion in the $D^{*+}\ell^-$ channel does not change the result by more than this uncertainty.

The uncertainty related to the dependence of the efficiency with ω corresponds to the change if the fit is performed with a linear instead of quadratic parameterization of the efficiency *vs* ω.

B **lifetimes:** A change in B^0 lifetime affects $\mathcal{F}(1)|V_{cb}|$ in two correlated ways. An increase in the lifetime directly decreases the partial width corresponding to a

fixed branching ratio. However the branching ratio also decreases because the requirement on the decay length above 1 mm favour long lifetime events. A change in the B^+ and B_s^0 lifetimes within errors also affects the proportion of physics background but this has a negligible effect on the final results.

7 Conclusion

The differential decay rates $d\Gamma/d\omega$ for the decays $\overline{B}^0 \to D^{*+}\ell^-\overline{\nu}_\ell$ and $\overline{B}^0 \to D^+\ell^-\overline{\nu}_\ell$ are measured. Using a linear ω dependence for the hadronic form factors $\mathcal{F}_{D^{*+}}(\omega)$ and $\mathcal{F}_{D^+}(\omega)$, the values of $\mathcal{F}_{D^{*+}}(1)|V_{cb}|$ and $\mathcal{F}_{D^+}(1)|V_{cb}|$ and of the slopes $a^2_{D^{*+}}$ and $a^2_{D^+}$ are:

$$\begin{aligned} \mathcal{F}_{D^{*+}}(1)|V_{cb}| &= (31.9 \pm 1.8_{stat} \pm 1.9_{syst}) \times 10^{-3} , \\ a^2_{D^{*+}} &= 0.31 \pm 0.17_{stat} \pm 0.08_{syst} , \end{aligned}$$

and

$$\begin{aligned} \mathcal{F}_{D^+}(1)|V_{cb}| &= (27.8 \pm 6.8_{stat} \pm 6.5_{syst}) \times 10^{-3} , \\ a^2_{D^+} &= -0.05 \pm 0.53_{stat} \pm 0.38_{syst} . \end{aligned}$$

The values of $\mathcal{F}_{D^{*+}}(1)|V_{cb}|$ and $a^2_{D^{*+}}$ are in agreement with the previous ALEPH measurement [6] updated for new D^0 branching ratios [19] and are more precise.

The ratio of the form factors $\mathcal{F}_{D^{*+}}(\omega)$ and $\mathcal{F}_{D^+}(\omega)$ at $\omega = 1$ and $\omega = \omega^{max}_{D^{*+}}$ and the difference of their slopes are measured to be

$$\begin{aligned} \frac{\mathcal{F}_{D^+}(1)}{\mathcal{F}_{D^{*+}}(1)} &= 0.87 \pm 0.22_{stat} \pm 0.21_{syst} , \\ \frac{\mathcal{F}_{D^+}(\omega^{max}_{D^{*+}})}{\mathcal{F}_{D^{*+}}(\omega^{max}_{D^{*+}})} &= 1.06 \pm 0.09_{stat} \pm 0.11_{syst}, \\ a^2_{D^+} - a^2_{D^{*+}} &= -0.36 \pm 0.58_{stat} \pm 0.31_{syst} . \end{aligned}$$

These measured values are in agreement with theoretical predictions from HQET. They represent the first direct tests of HQET prediction of the universality of the Isgur-Wise function.

$|V_{cb}|$ is usually derived from $\mathcal{F}_{D^{*+}}(1)|V_{cb}|$, although the linear parameterization of the form factor is arbitrary. It is however possible to use a quadratic parameterization of the form factor with only a small loss of precision using theoretical relations between the slope and curvature of the hadronic form factors and their calculated values at $\omega = 1$. $|V_{cb}|$ and the slope of the Isgur-Wise function are then measured to be

$$\begin{aligned} |V_{cb}| &= (34.4 \pm 1.6_{stat} \pm 2.3_{syst} \pm 1.4_{th}) \times 10^{-3} , \\ a^2_0 &= 0.30 \pm 0.12_{stat} \pm 0.14_{syst} \pm 0.13_{th} . \end{aligned}$$

The integrated spectra of the two semileptonic B^0 decay channels yield the following branching fractions:

$$\begin{aligned} Br(\overline{B}^0 \to D^{*+}\ell^-\overline{\nu}_\ell) &= (5.53 \pm 0.26_{stat} \pm 0.52_{syst})\% , \\ Br(\overline{B}^0 \to D^{+}\ell^-\overline{\nu}_\ell) &= (2.35 \pm 0.20_{stat} \pm 0.44_{syst})\% . \end{aligned}$$

Acknowledgements

We are grateful to Irinel Caprini, Laurent Lellouch and Matthias Neubert for useful discussions. We wish to thank our colleagues from the accelerator division for the successful operation of LEP. We are indebted to the engineers and technicians at CERN and our home institutes for their contribution to the good performance of ALEPH. Those of us from non-member countries thank CERN for its hospitality.

References

[1] M.B. Voloshin and M.A. Shifman, Sov. J. Nucl. Phys. 47 (1988) 511.

[2] N. Isgur and M.B. Wise, Phys Lett. B 232 (1989) 113; *ibid* 237 (1990) 527.

[3] M. Neubert, Phys. Rep. 245 (1994) 259.

[4] H. Albrecht et al. (ARGUS Coll.), Phys. Lett. B 197 (1989) 452;
H. Albrecht et al. (ARGUS Coll.), Phys. Lett. B 275 (1992) 195;
H. Albrecht et al. (ARGUS Coll.), Z. Phys. C 57, (1993) 533;
H. Albrecht et al. (ARGUS Coll.), Phys. Lett. B 324 (1994) 249.

[5] D. Bortoletto et al. (CLEO Coll.), Phys. Rev. Lett. 63, (1989) 1667;
R. Fulton et al. (CLEO Coll.), Phys. Rev. D 43, (1991) 651;
B. Barish et al. (CLEO Coll.), Phys. Rev. D 51 (1995) 1014.

[6] D. Buskulic et al. (ALEPH Coll.), Phys. Lett. B 359 (1995) 236.

[7] P. Abreu et al. (DELPHI Coll.), "Determination of $|V_{cb}|$ from the semileptonic decay $\overline{B}^0 \to D^{*+}\ell^-\overline{\nu}_\ell$", CERN-PPE/96-011 (1996), submitted to Z. Phys. C.

[8] M. Neubert, Phys. Lett. B 264 (1991) 455.

[9] I. Caprini and M. Neubert, Phys. Lett. B 380 (1996) 376.

[10] Z. Ligeti, Y. Nir and M. Neubert, Phys. Rev. D 49 (1994) 1302.

[11] D. Decamp et al. (ALEPH Coll.), Nucl. Instr. and Meth. A 294 (1990) 121;
D. Buskulic et al. (ALEPH Coll.), Nucl. Instr. and Meth. A 346 (1994) 461.

[12] D. Buskulic et al. (ALEPH Coll.), Nucl. Instr. and Meth. A 360 (1995) 481.

[13] D. Decamp et al. (ALEPH Coll.), Z. Phys. C 53 (1992) 1.

[14] D. Buskulic et al. (ALEPH Coll.), Phys. Lett. B 357 (1995) 699.

[15] D. Buskulic et al. (ALEPH Coll.), Phys. Lett. B 357 (1995) 699.

[16] D. Buskulic et al. (ALEPH Coll.), "Production of orbitally excited charm mesons in semileptonic B decays", CERN-PPE/96-092 (1996), submitted to Z. Phys. C.

[17] D. Buskulic et al. (ALEPH Coll.), Phys. Lett. B 343 (1995) 444.

[18] D. Buskulic et al. (ALEPH Coll.), "Study of double charmed B decays at LEP", Contribution PA05-060 to the 28th International Conference on High Energy Physics, Warsaw, Poland, 25-31 July 1996.

[19] R.M. Barnett et al., "Review of Particle Physics", Phys. Rev. D 54 (1996) 1.